# MEASUREMENTS OF ERTEL VORTICITY FINESTRUCTURE IN THE EASTERN NORTH ATLANTIC

Eric Kunze
School of Oceanography, University of Washington, WB-10, Seattle, WA 98195

Thomas B. Sanford
Applied Physics Laboratory, HN-10, University of Washington, Seattle, WA 98105

## ABSTRACT

Two velocity and temperature profile surveys collected near Ampere Seamount in the eastern North Atlantic reveal ertel vorticity finestructure on horizontal scales of 3-7 km and vertical wavelengths of 40-400 m (Burger numbers of 0.05-30). Just as on basin scales, this finescale ertel vorticity signal is dominated by stretching. The dynamic signal, as characterized by the relative vorticity and horizontal convergence, is consistent with the GM internal wave model and is dominated by near-inertial waves on the resolved scales. The dominance of stretching indicates that ertel vorticity finestructure is associated with passive density finestructure of very low aspect ratio. This suggests that it was not formed recently by flow separation at the seamount but might be an artifact of subduction of surface mixed layers or injection of benthic boundary layers into the pycnocline.

## INTRODUCTION

At the large wavelengths that dominate horizontal velocity and vertical displacement in the ocean interior, fluctuations are largely linear, allowing identification of subinertial frequency flows as quasigeostrophic and superinertial motions as internal gravity waves. But at high wavenumbers, advective nonlinearity acts to Doppler shift and alias variance across frequency space, making identification of dynamics from Eulerian frequency impossible; many intrinsic frequencies will contribute to the same Eulerian frequency. Given that the aspect ratios of the dominant finescale motions are $\leq f/N \simeq 0.01$ (Marmorino *et al.*, 1987; Gregg *et al.*, 1986, Itsweire *et al.*, 1989), vertical advection by low-mode internal waves should be the main perpetrator of advective nonlinearity.

Using current-meter and temperature time-series from the IWEX trimooring array, Briscoe (1977) and Müller *et al.* (1978) found finestructure in the internal-wave frequency band with amplitudes of 2 cm $s^{-1}$ and vertical scales of 2 m that contained too much velocity relative to temperature variance to be explained by linear internal wave dynamics. Excess finescale velocity in the continuum frequency band was also reported by Eriksen (1978). Kunze *et al.* (1990) confirmed this result and found excess strain in the near-inertial band. For linear internal waves, the shear-to-strain ratio $V_z/(N\zeta_z) = 1$ at intermediate intrinsic frequencies, $f << \omega_o << N$. As $\omega_o \rightarrow f$, this ratio approaches infinity while as $\omega_o \rightarrow N$, it approaches zero. Müller *et al.* (1978) also found that the vertical coherence scale for velocity was smaller than for temperature. Two sets of dynamics have

been proposed to explain the velocity finestructure: stratified two-dimensional turbulence (vortical mode) (Holloway, 1983; Müller, 1984) and near-inertial waves (Kunze *et al.*, 1990). Near-inertial waves dominate variance at larger scales (e.g., Garrett and Munk, 1979). Kunze *et al.* demonstrated that the finestructure properties were consistent with a finescale internal wave spectrum dominated by near-inertial waves. Resolving the dynamics of the finescale has important implications for stirring and mixing of water properties.

Stratified two-dimensional turbulence is the stratified, nonlinear analog of two-dimensional quasigeostrophic turbulence (Riley *et al.*, 1981; Lilly, 1983; Müller, 1984). Such motion would have subinertial intrinsic frequencies. Müller (1984) referred to stratified two-dimensional turbulence as 'vortical mode' because ertel vorticity anomalies can be associated with it while internal gravity waves can have no ertel vorticity fluctuations associated with them. Following a water parcel, ertel vorticity can only be modified by irreversible processes (Ertel, 1942; Pedlosky, 1978; Haynes and McIntyre, 1986). For example, Lelong and Riley (1991) have shown that wave/wave and wave/vortex interactions do not modify ertel vorticity. Thus, while internal waves can carry energy into the ocean interior, ertel vorticity anomalies are tied to a water parcel. Vortices have been observed in laboratory stratified-wake experiments (Lin and Pao, 1979) and as a decay product in numerical simulations of dissipative turbulence (Riley *et al.*, 1981; Staquet and Riley, 1989; Herring and Metais, 1989). They also appear in numerical simulations of 'forced internal waves' if the forcing projects on ertel vorticity anomalies (Metais and Herring, 1989; Holloway and Ramsden, 1990). Metais and Herring found that a numerically simulated field of random internal waves without ertel vorticity anomalies did not create vortical mode. Because turbulence and mixing are weak and confined to small vertical scales in the ocean interior (Moum and Osborn, 1986; Gregg, 1987; Gregg, 1989; Yamazaki *et al.*, 1990), we anticipate that ertel vorticity anomalies produced there to be likewise weak and confined to small vertical scales where molecular viscosity will rapidly eliminate any dynamic signal. However, considerable finestructure may be generated in regions of strong forcing, such as at boundaries, and survive little affected as it is carried into the ocean interior by subduction. The question of what fractions of finescale variance in the ocean are internal waves and stratified two-dimensional turbulence can only be answered with measurements.

A first attempt to estimate ertel vorticity on the finescale was undertaken by Müller *et al.* (1988). Using the IWEX array velocity measurements, they estimated the relative vorticity directly and stretching from the time-integral of horizontal convergence. The vorticity and convergence spectra were identical. Kunze *et al.* (1990) questioned their claim of having found an ertel vorticity signal on the grounds that (i) like quasigeostrophic flow, vortical mode should have little or no horizontal convergence so their 'stretching' signal was internal wave strain, (ii) near-inertial internal waves have vorticity as well as convergence, and (iii) in a blue spectra, a three-point array will detect 'vorticity' even in a pure convergence field and vice versa. Lien (1990) illustrated that this can explain the large horizontal scales from IWEX. But at radii of 25 m, the IWEX-aliased GM vorticity lies below GM convergence unlike the measurements. On these scales, GM isopycnal slopes tilt vertical shear into vertical vorticity sufficiently to explain the measurements. Thus, the IWEX measurements of velocity finestructure are explicable as internal waves, and Müller *et al.*'s (1988) conclusion that they identified ertel vorticity finestructure is suspect.

Using measurements from a neutrally buoyant float, Kunze *et al.* (1990) showed that, given typical finescale aspect ratios $\leq f/N \simeq 0.01$ (Marmorino *et al.*, 1987; Gregg *et al.*, 1986, Itsweire *et al.*, 1989), the observed finescale shear-to-strain ratio of 2.2 was too high to be explained by stratified two-dimensional turbulence. However, it was consistent with a finescale internal wave spectrum dominated by near-inertial waves. Indeed, the observed shear-to-strain ratio is only slightly above the GM value of 1.7 (Munk, 1981). The semi-Lagrangian strain spectra of Sherman and Pinkel (1991) supports the interpretation that most shear variance at high wavenumber is Doppler-smeared near-inertial motions rather than vortical mode. In contrast, D'Asaro and Morehead (1991) found that the incoherent signal at 40-m vertical wavelength in velocity profile surveys had a potential-to-horizontal kinetic energy ratio (*PE/HKE*) and Burger number ($N^2k_H^2/f^2k_z^2$) consistent with vortical mode and not internal wave dynamics (Fig. 1). These measurements were collected under the ice in the Beaufort Sea. The incoherent (vortical) signal contained as much energy as the high-frequency internal waves in the weak internal wave regime under the ice. None of these measurements were able to estimate ertel vorticity.

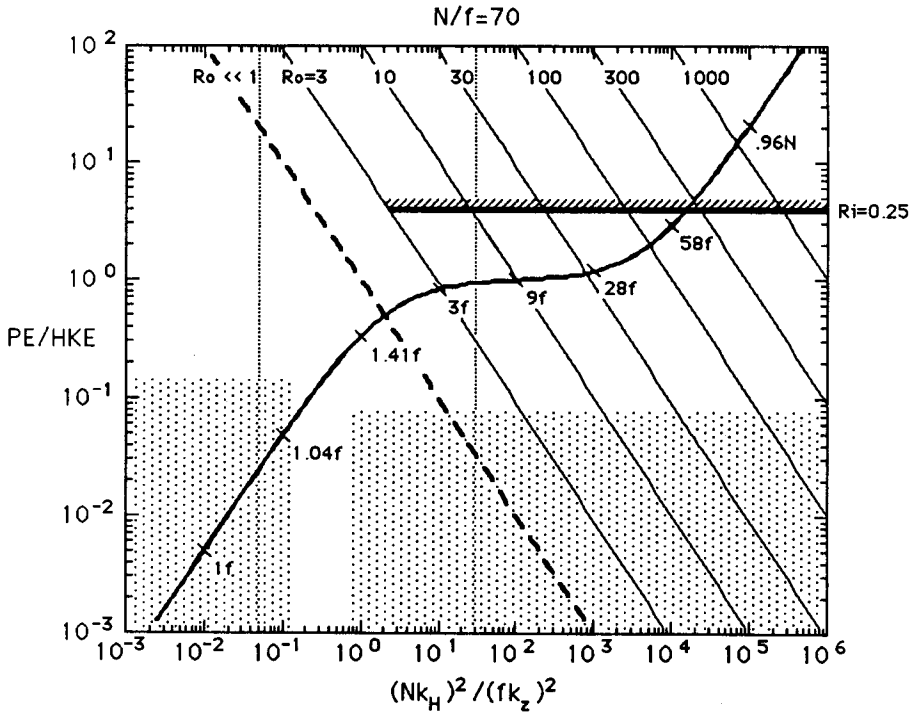


Figure 1. A dynamic diagram of the ratio of potential-to-horizontal kinetic energy *PE/HKE* versus Burger number $(N^2k_H^2)/(f^2k_z^2)$ from D'Asaro and Morehead (1991). The *S*-curve is the consistency relation (marked with intrinsic frequencies) for internal waves with $N/f = 70$ [$PE/HKE = B/(B+2)$]. The thick-dashed diagonal corresponds to geostrophy [$PE/HKE = 1/B$] and the thick solid diagonals to high Rossby number vortical mode [$PE/HKE = Ro^2/B = 1/Ri$]. The two blocks of stippling correspond to the coherent signal (left), which is in the near-inertial wave part of the diagram, and the incoherent signal (right), which is in the geostrophic/ vortical regime, from D'Asaro and Morehead's XCP surveys in the Beaufort Sea. The two vertical dotted lines bound the Burger numbers resolved by the Ampere Seamount surveys.

In September 1988, an expedition was made to Ampere Seamount at 35° 03.5' N, 12° 52.2' W in the eastern North Atlantic (Fig. 2) to look for evidence of ertel vorticity finestructure which would be a signature of stratified two-dimensional turbulence. The Coriolis frequency at this latitude is $8.3 \times 10^{-5}$ s $^{-1}$ It was thought that the likelihood of finding this signal would be greater in the vicinity of a seamount where flow separation might lead to shed eddies in the wake. However, as no finescale ertel vorticity measurements have been made in the ocean, this was not crucial. Eddy-shedding did not appear to be playing a role in the data we collected.

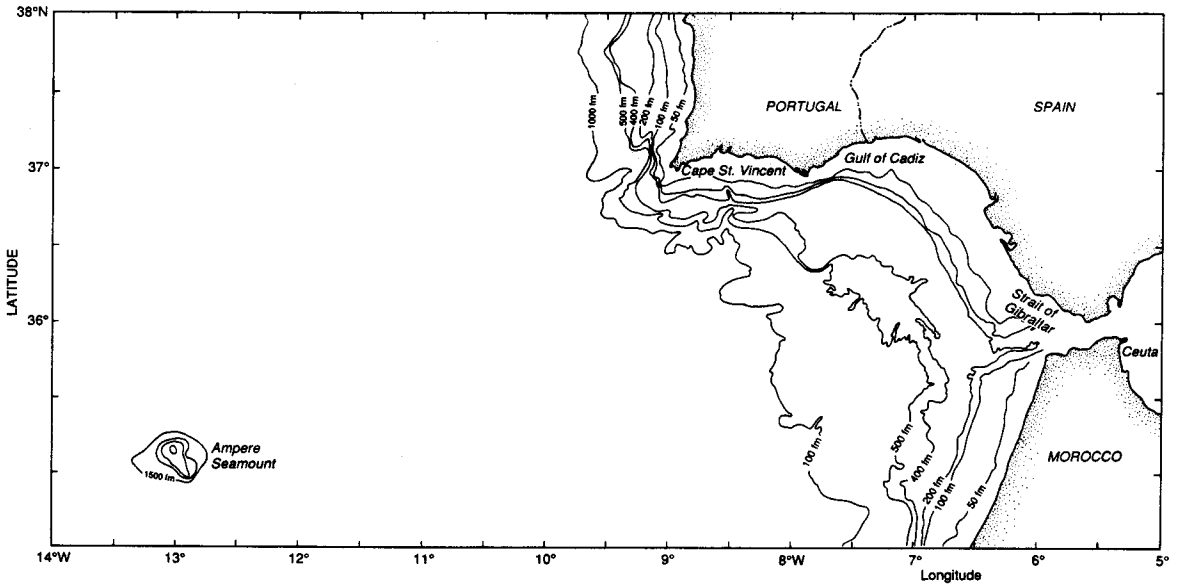


Figure 2. Bathymetry in the eastern North Atlantic showing the location of Ampere Seamount at 35° 04'N, 12° 52'W outside the mouth of the Gulf of Cadiz. The summit comes within 53 m of the surface.

## MEASUREMENTS

We first undertook an XBT box survey 60 km on a side around the seamount (Fig. 3) to look for mesoscale impinging geostrophic flow. No signal was apparent. Four drifters were then deployed within 10 km of the summit to examine the near-field mean flow. Three of these drifters were recovered and redeployed on the eastern flank for a total of seven drifter tracks. The drifters were drogued to 100-200 m using a high-drag line in that depth range and a low-drag line to the surface (Drever and Kennelly, 1991). Radar reflectors were used to locate the drifters. The ship came alongside each drifter to determine its range and bearing to a radar beacon moored on the summit (Fig. 3). Range is accurate to ±200 m and bearing to ±2°. Positioning based on Loran C was good to one kilometer in $x$ and $y$. The drifters were tracked from 6-10 September 1988. On the northern flank of the seamount and to the east in an interior boundary layer, drifters 1 and 2 moved persistently toward the east with average speeds of 5-7 cm s$^{-1}$ (Fig. 4). Tidal fluctuations of ±5 cm s$^{-1}$ were also primarily in the $u$ velocity component. On the eastern flank, motion was

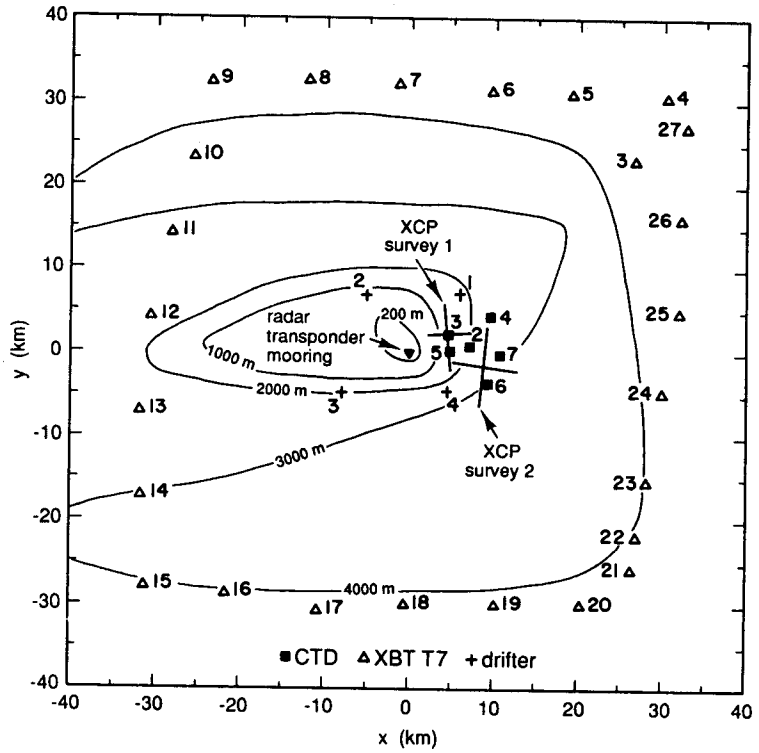


Figure 3. Sampling in the neighborhood of Ampere Seamount including an XBT box survey (Δ) around the seamount, drifter deployments (+) tagged to 100-200 m depth, six CTD casts (❑) and two cross-shaped XCP surveys on the eastern flank. The XCP surveys contained 27 and 28 profiles at spacings of 0.3-1 km. A radar transponder navigation mooring was located on the summit (∇).

weak and random for the first three days, then accelerated to the south during 9 September, reaching speeds of ~10 cm $s^{-1}$. Drifter 3, deployed southwest of the summit, moved southward at ~13 cm $s^{-1}$. However, on recovery it was discovered to have lost its drogue so its track is not representative of the flow at 100-200 m depth. The last drifter was recovered in the middle of 9 September.

Based on the lateral shear between drifters on the northern and eastern flanks of Ampere Seamount during the first three days of the drifter deployment (Fig. 5), which correspond to vorticities ~0.5*f*, it was thought that flow separation was most likely to occur in the northeast corner of the summit. Eddies generated by this mechanism would be found east and north of the summit so two cross-shaped finescale expendable current profiler (XCP) surveys were conducted near the northeast flank on the afternoons of 8 and 9 September (Fig. 3). Six CTD casts to 2000-m depth were made here between the XCP surveys to determine the local $T,\sigma$–relation. The XCP surveys contained 28 and 27 probes with 12 to 14 XCPs in each leg and drop spacings of 0.3-1 km. Survey 1 was effectively 4 km in diameter and survey 2 was 7 km across. Each survey was completed in three hours in an effort to minimize biasing of the spatial gradients by temporal variability. Because these horizontal scales are dominated by near-inertial waves, this appears to have been effective. Vertical wavenumber spectra of profile sums and differences near the intersection of the legs suggest that temporal variability has little impact on wavelengths greater than 100 m.

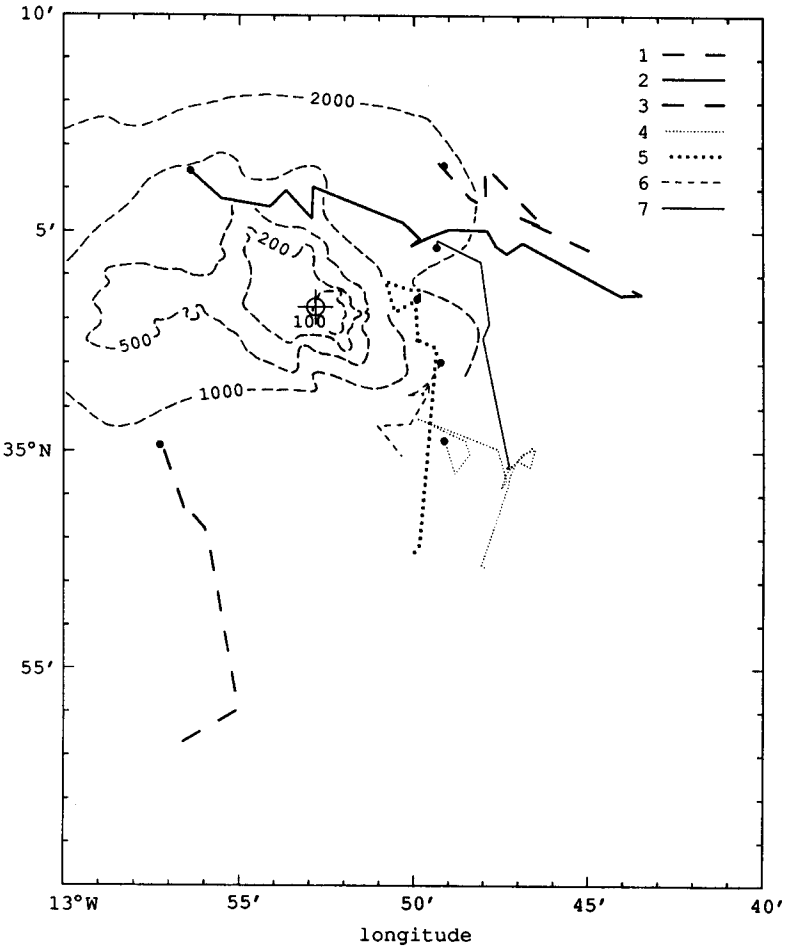


Figure 4. The seven drifter tracks span 6 to 10 September superimposed on Ampere Seamount bathymetry. Drifters on the northern flank of Ampere moved eastward at 5-7 cm $s^{-1}$, extending off the flank in an interior boundary layer to the east. Those on the eastern flank moved little for the first three days, then moved southward at speeds exceeding 10 cm $s^{-1}$. The drifter to the southwest moved south at 13 cm $s^{-1}$ but it lost its drogue.

Expendable current profilers electromagnetically measure the horizontal velocity ($u$ , $v$) relative to a depth-independent constant (e.g., measures the baroclinic flow) and measure temperature $T$ with an XBT thermistor. Data values are recorded every 0.3 m from the surface to ~1600-m depth. The upper 50 m is generally contaminated by temporally aliased velocities associated with the surface swell. In the pycnocline, the oceanic signal typically falls below the instrumental noise level for wavelengths smaller than 10 m. Therefore, standard pre-analysis XCP processing smooths the raw data with a 6-m triangular window every 3 m. The velocities have rms errors of ±0.4 cm $s^{-1}$ and temperature errors of ±0.15 °C. We will be using these data to compute vertical and horizontal gradients. The velocity error corresponds to shear errors of $\pm 10^{-4}$ $s^{-1}$ ~ $0.03N$ over 40 m (vertical) and $\pm 10^{-6}$ $s^{-1}$ ~ $0.013f$ over 4 km (horizontal). The temperature error corresponds to $\pm 4 \times 10^{-3}$ °C $m^{-1}$ ≡ $4 \times 10^{-6}$ $s^{-2}$ ~ $0.3N^2$ over 40 m and $\pm 4 \times 10^{-5}$ °C $m^{-1}$ ≡ $4 \times 10^{-8}$ $s^{-2}$ ~$0.15fN$ over 4 km given $\partial b/\partial T \sim 10^{-3}$ m $s^{-2}$ °$C^{-1}$. Thus, with comparison to $f$ and $N$, the velocity contributes smaller errors to an ertel vorticity signal (see below) than temperature. Assuming resolved vertical scales of 40-400 m and horizontal scales of 3-7 km , the range of resolved Burger number is 0.05-30 (between the dotted vertical lines in Fig. 1). For internal wave dynamics, this range includes frequencies up to $3f$. For vortical dynamics, Rossby numbers up to ten are in principle measurable.

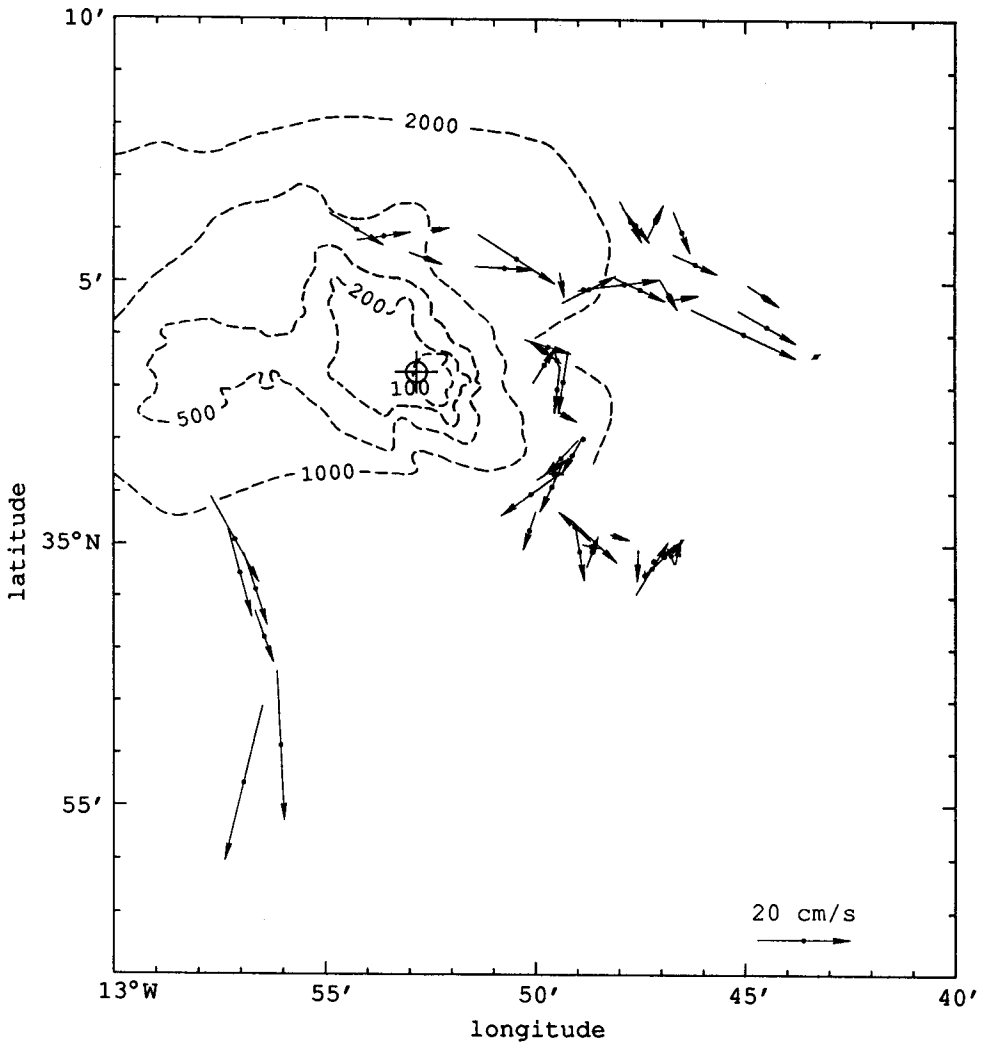


Figure 5. Drifter velocities around Ampere Seamount for the period prior to the acceleration to the south on the eastern flank.

## ERTEL VORTICITY

### *Review*

Following a water parcel, the ertel vorticity cannot be modified except by irreversible processes: external forcing, dissipative turbulence and mixing (Ertel, 1942; Pedlosky, 1978). Thus, no ertel vorticity fluctuations are associated with nondissipative internal waves. For linear internal waves, the linear stretching and relative vorticity contributions to ertel vorticity are equal and opposite. At high wavenumbers where nonlinearity becomes important, nonlinear contributions of the ertel vorticity may contribute, but no total ertel vorticity anomalies arise in the absence of internal wave dissipation (Lelong and Riley, 1991).

The ertel vorticity will be defined here as the dot product of the total vorticity ($2\Omega + \nabla \times V$) and the gradient of the buoyancy $\nabla(\bar{B} + b)$

$$\Pi = (2\Omega + \nabla \times V)\cdot\nabla(\bar{B} + b) \qquad (1)$$

where Earth's rotation, $2\Omega = (0, 2\Omega\cos(lat^\circ), 2\Omega\sin(lat^\circ)) = (0, f\cot(lat^\circ), f)$, and the buoyancy $\bar{B} + b = -g\delta\rho/\rho_O$ has been split into a largescale background $\bar{B}(z)$ varying only with depth and smaller scale anomalies $b(x,y,z,t)$. The splitting of the vertical buoyancy gradient is not necessary but is common practice and a convenient way of separating large and small scales. Neglecting the meridional component of Earth's rotation and the vertical velocity $w$, Eq. (1) can be expanded into a background, linear and nonlinear part

$$\Pi = f\bar{N}^2 + fb_z + (v_x - u_y)\ \bar{N}^2 + (v_x - u_y)b_z - b_x v_z + b_y u_z \qquad (2)$$

(i) (ii) (iii) (iv) (v) (vi)

where subscripts denote derivatives and $\bar{N}^2 = \partial\bar{B}/\partial z$ is the background buoyancy frequency. The background ertel vorticity (i) involves only the smoothed stratification $\bar{B}(z)$ and the planetary vorticity $f$. The linear ertel vorticity anomaly is made up of buoyancy-gradient anomalies (ii) and relative vorticity (iii). Nonlinear ertel vorticity anomalies arise from coupling of buoyancy-gradient anomalies and relative vorticity (iv) and the twisting terms (v) and (vi).

*Data*

Estimating the different components of (2) requires determination of both horizontal and vertical gradients of $u$, $v$ and $b$. This is achievable with cross-shaped XCP surveys provided that the surveys are coherent so that (i) horizontal gradients can be estimated and (ii) temperature can be used as a proxy for buoyancy.

To demonstrate that the survey was coherent, Fig. 6 displays the eastwest section of east velocity $u$ from survey 2. Fluctuations of $\pm 10$ cm s$^{-1}$ are seen on scales of tens to hundreds of meters with vertical structure down to scales of 50 m coherent across much of the transect. Vertical least-squares cubic fits to the profiles (dashed lines) reveal little variance associated with vertical wavelengths greater than 1000 m. As wavelengths ~1000 m can be affected by the barotropic offset when profiles are not of identical length and our main interest here is in the finescale ($\lesssim 100$ m), the cubic fits were removed before subsequent analysis. Because the profiles are horizontally coherent, we are justified in estimating the horizontal gradients $\partial/\partial x$ from the eastwest legs and $\partial/\partial y$ from the northsouth legs using least-squares fits. These are then combined to determine dynamically relevant variables. Figure 7a displays the relative vorticity $(v_x - u_y)/f$ for survey 1 as a function of depth $z$ and the horizontal scale over which the fit was performed $\Delta r$. As the fitting scale $\Delta r$ increases, so does the number of profiles going into the fit (number at bottom of each profile) while the standard deviation (stippling), as determined using a bootstrap technique, decreases. At $\Delta r$=4 km , the relative vorticity has significant fluctuations on scales of tens to

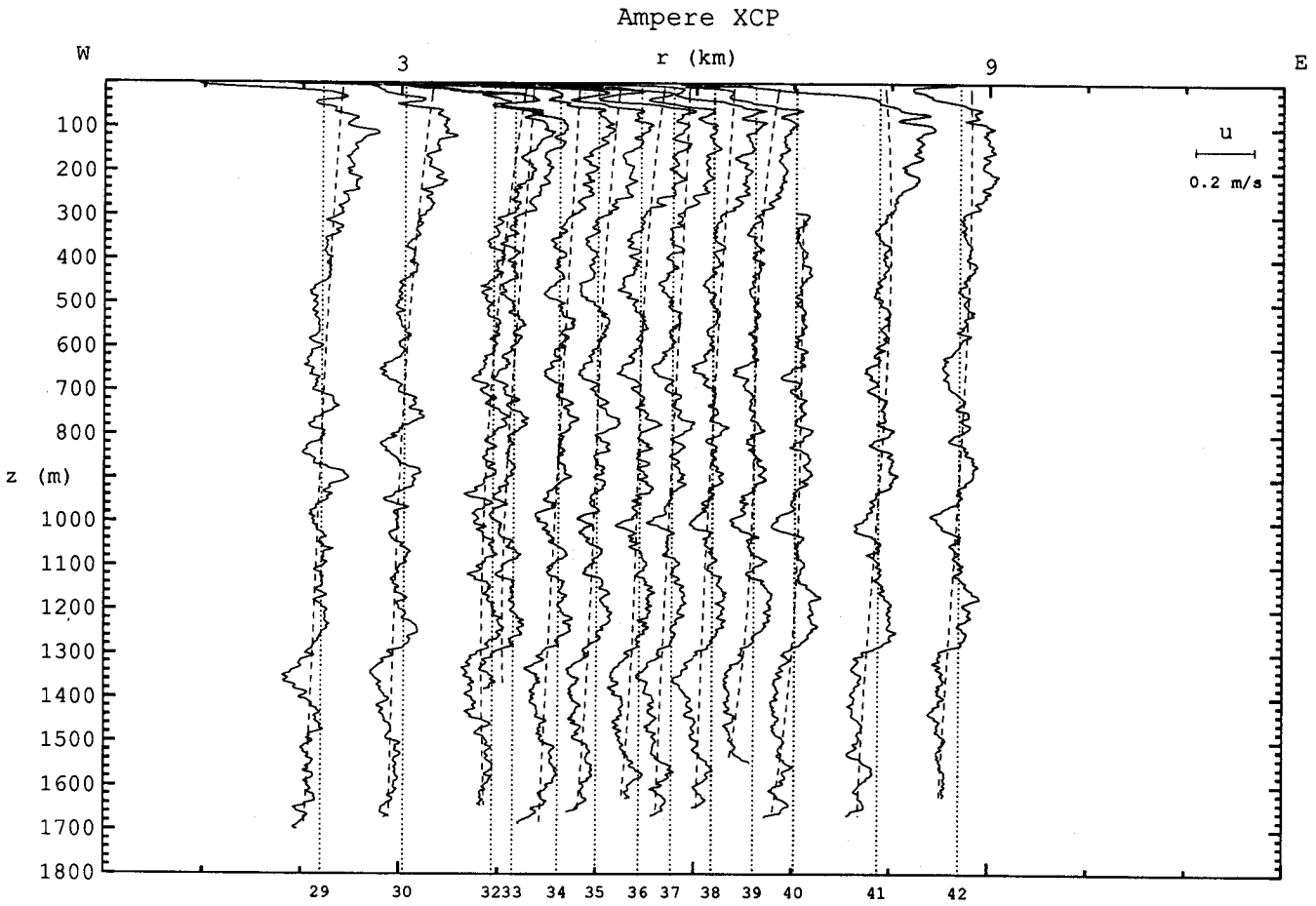


Figure 6. A sample section of $u$ velocity profiles from the east-west leg of XCP survey 2. The dashed lines indicate cubic fits to the profiles. Fluctuations coherent over much of the transect are evident down to scales of tens of meters.

hundreds of meters with rms values of 0.2-0.3$f$, an order of magnitude above instrument noise. Unresolved oceanic variance is ~0.1$f$. The horizontal convergence $(u_x + v_y)/f$ for survey 1 (Fig. 7b) has similar characteristics. Inertially rotating the velocity profiles to a common time before carrying out the fits did not alter the details of the vorticity and convergence profiles appreciably.

Figure 8 displays the $T,\sigma$–relation from the CTD casts collected near the seamount. The relation is tight for temperatures $T < 10$ °C (depths greater than 1250 m) and for 12 °C $< T <$ 16 °C (150-600 m depth) but not in the salt-stratified isothermal layer between 600 and 1200 m, nor in the upper 150 m where water-mass gradients are evident. In this paper we will confine our attention to 150-600 m depth and use $b(T) = T \cdot \partial b/\partial T$ based on least-squares fits to the CTD data to relate buoyancy to temperature. For 150-600 m depth, $\partial b/\partial T \simeq 10^{-3}$ m s$^{-2}$ °C$^{-1}$ and the buoyancy frequency $\bar{N} = 3.3\text{-}3.8 \times 10^{-3}$ s$^{-1}$.

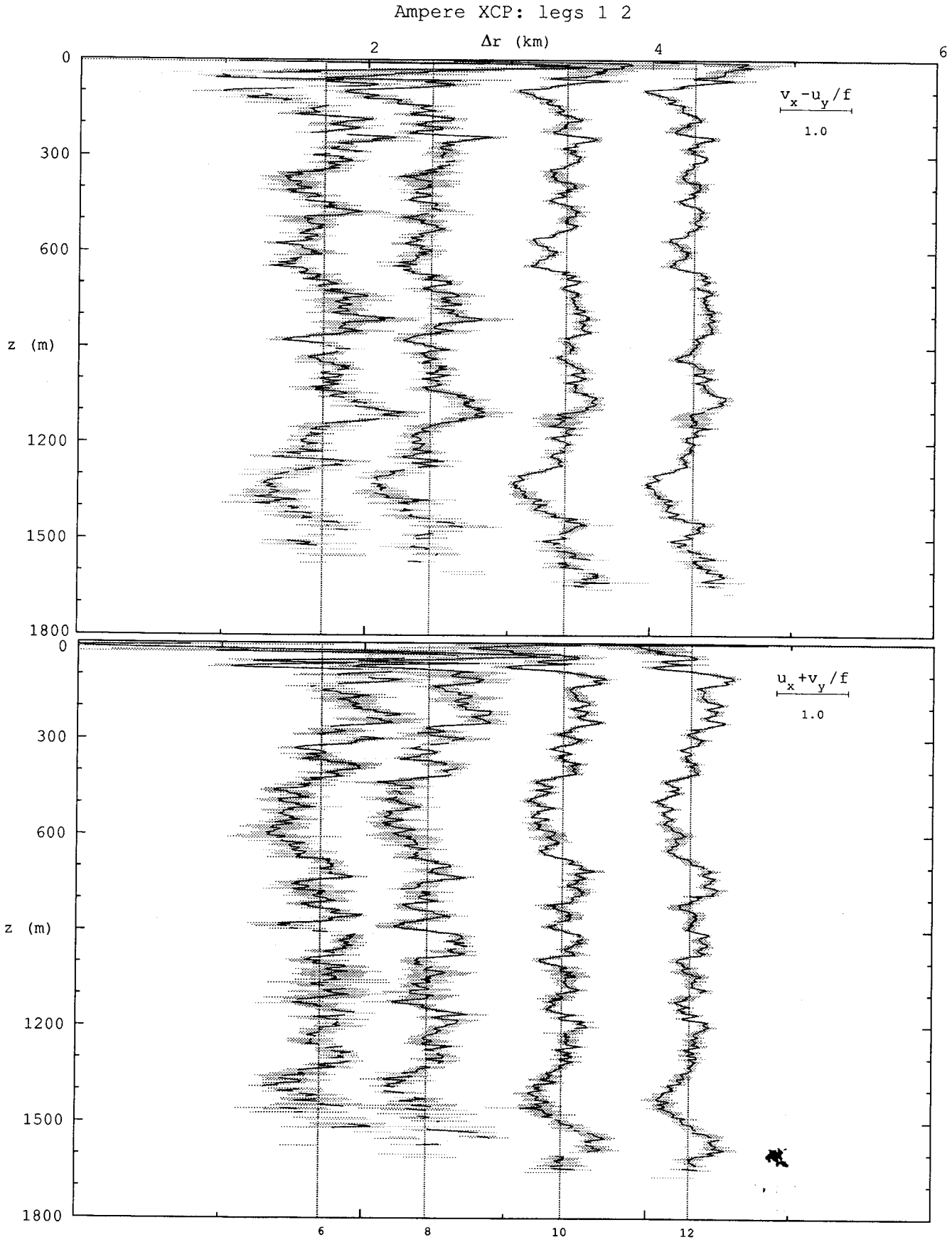
Ampere XCP: legs 1 2
Δr (km)
2
4
6
0
300
600
z (m)
1200
1500
1800
$v_x - u_y / f$
1.0
$u_x + v_y / f$
1.0
6
8
10
12

Figure 7a. (Facing page, top) Survey 1 relative vorticity $(v_x - u_y)/f$ from least-squares horizontal fits as function of depth $z$ and the fitting scale $\Delta r$. As the fitting scale increases, the number of drops in the fit increases (numbers at bottom of each profile) and the standard deviation (stippling) diminishes. For a fitting scale $\Delta r = 4$ km , significant fluctuations occur on scales greater than 50 m with rms values of 0.2-0.3$f$.

Figure 7b. (Facing page, bottom) As in Fig. 7a but for horizontal convergence $(u_x + v_y)/f$. Magnitudes and scales are comparable to those of relative vorticity.

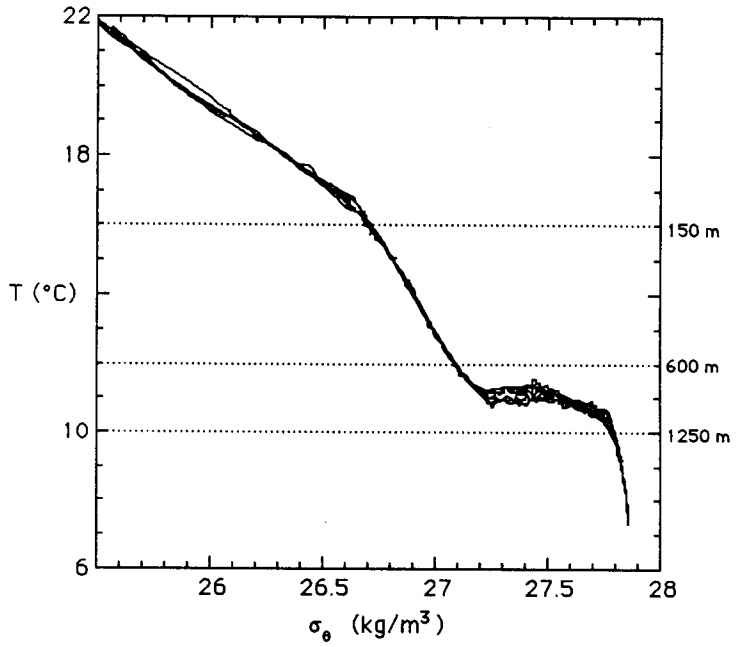


Figure 8. Temperature $T$ versus density $\sigma_t$ from the six CTDs collected east of Ampere. For temperatures less than 10 °C (depths greater than 1250 m) and between 12-16 °C (150-600 m), the $T,\sigma$-relation is tight, allowing temperature to be used as a proxy for buoyancy (density). A salt-stratified isothermal layer occupies the depth range 650-1200 m and water-mass gradients are evident in the upper 150 m.

*Spectra*

The sum of the five linear and nonlinear terms of the ertel vorticity (2) reveals that there is ertel vorticity finestructure present between 150- and 600-m depth. The nonlinear terms contribute little to the signal, that is, on the scales of the survey, the ertel vorticity is linear. The stretching term dominates. These results are most clearly seen in vertical wavenumber spectra of the ertel vorticity terms (Fig. 9). The spectra are presented in both log-log and variance-preserving forms. Figure 9a displays the ertel vorticity component spectra for survey 1 and a fitting scale $\Delta r$=4 km and Fig. 9b for survey 2 and $\Delta r$=7 km. The stretching $fb_z$ (thick solid) clearly dominates the variance, peaking at 50-100 m wavelength. This scale is at least in part due to the horizontal averaging over the fitting scale which smooths over higher wavenumbers. The nonlinear terms are at least an order of magnitude smaller at all wavenumbers. The other linear term, the vorticity $\zeta \bar{N}^2$, is an order of magnitude smaller than the stretching at 50-100 m wavelength but comparable in magnitude at lower wavenumbers. It exceeds stretching in the lowest wavenumber band in the second survey but this is a consequence of the cubic-fit separation of background $\bar{N}^2$ and anomaly $b_z$ which

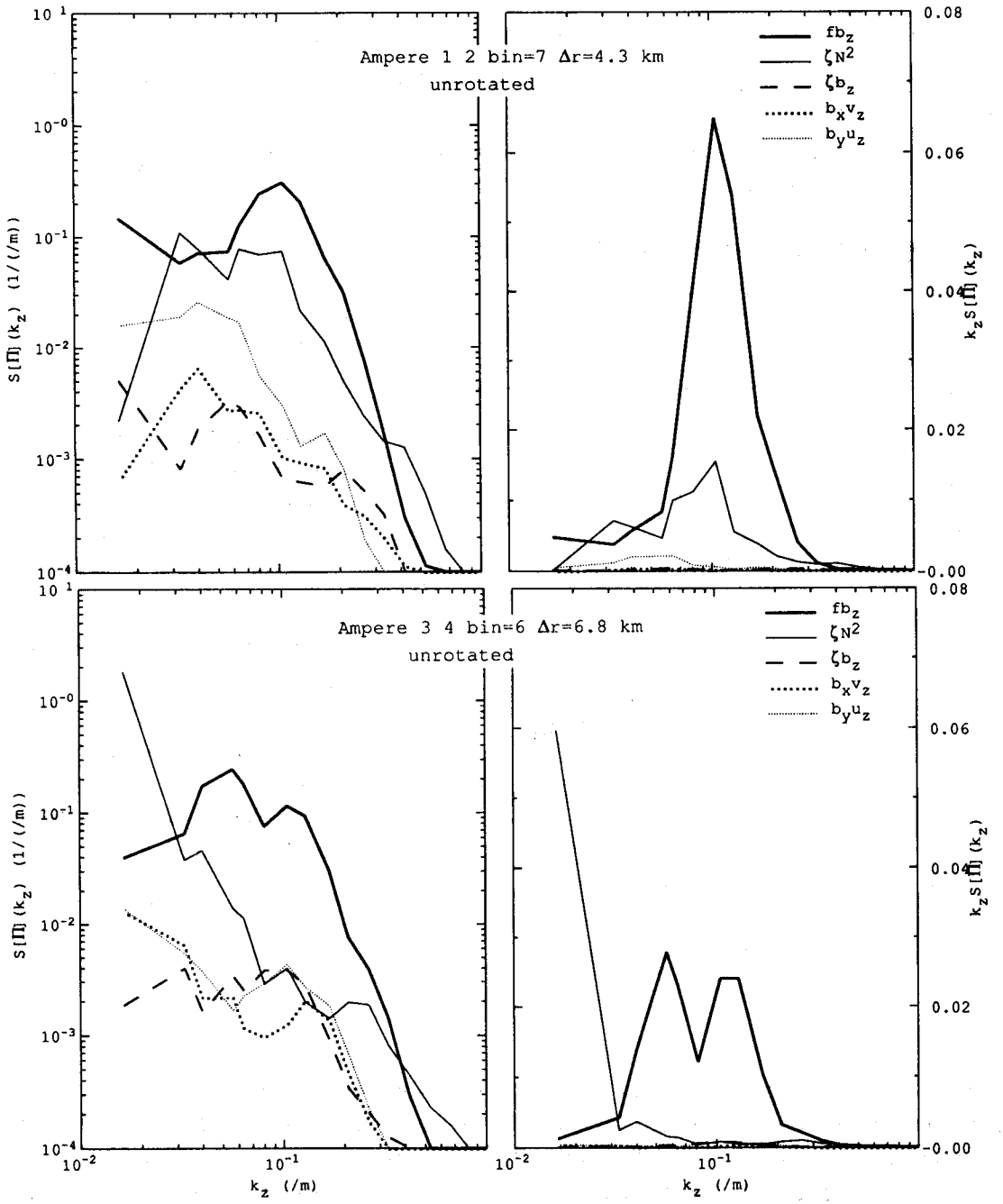


Figure 9. (a, top) Vertical wavenumber spectra from survey 1 with horizontal fitting scale $\Delta r = 4$ km for the linear and nonlinear terms in the ertel vorticity (2) including stretching $fb_z$, vorticity $(v_x - u_y)\,\bar{N}^2$, $(v_x - u_y)b_z$, and twisting $b_x v_z$ and $-b_y u_z$ terms. The spectra are presented in both log-log (left) and variance-preserving (right) forms. The stretching peak at 60-m wavelength contains an order of magnitude more variance than the other terms. At lower wavenumbers ($\lambda_z > 100$ m ), vorticity and stretching become comparable. At higher wavenumbers ($\lambda_z < 20$ m) vorticity slightly exceeds stretching due to the 12-m scale over which vertical gradients were computed. (b, bottom) As in Fig. 9a but for survey 2 with 7-km fitting. The stretching excess peak ranges from $\lambda_z = 30$-160 m. Vorticity exceeds stretching at the lowest resolved wavenumber as a consequence of the cubic fit used to separate $\bar{N}^2$ and $fb_z$.

assigns all low wavenumber variance to the background. At high wavenumbers, vorticity exceeds stretching because of the 12-m scale over which first-differencing to estimate $b_z$ was performed.

Comparing the measured stretching (strain) and vorticity spectra with the GM model (Figs. 10 and 11) reveals that, while the stretching greatly exceeds the GM model in the 50-100 m wavelength band, the vorticity spectra are comparable to GM (for this comparison, the high horizontal wavenumbers that the array does not resolve have been eliminated from the GM model with a simple boxcar lowpass filter with a cutoff $k_H = \pi/\Delta r$). In survey 1, the vorticity has a weak peak at 50-100 m but is generally similar in shape and level to GM. In survey 2, the vorticity lies on the GM model except at the largest resolved vertical wavelength ($\lambda_z$ = 384 m). Thus, while stretching greatly exceeds vorticity indicating the presence of vortical mode, the dynamic (velocity) signal differs little from the GM model. This suggests that the velocity signal could be predominantly due to internal waves. This can be tested by comparing the measured vorticity and convergence fields with the filtered GM model (Fig. 12). For survey 1 and $\Delta r$= 4 km , the observations share with the GM model the tendency for (i) convergence to exceed vorticity at low vertical wavenumbers, (ii) convergence and vorticity to be nearly identical at high vertical wavenumbers, and (iii) convergence to peak at slightly lower wavenumbers than vorticity. The same cannot be said of survey 2 where vorticity slightly exceeds convergence at most wavenumbers. This is *not* consistent with internal-wave dynamics for which $(\nabla_H \cdot V) \geq (\nabla_H \times V)$. We caution that the difference between the two spectra is small and may not be significant. If this is the case, the survey 2 spectra suggest a larger relative contribution from near-inertial waves [for which $(\nabla_H \cdot V) \simeq (\nabla_H \times V)$] than the GM model and survey 1.

For survey 1, for which the convergence exceeds the vorticity at most wavenumbers, consistent with internal-wave dynamics, the ratio of these two quantities can be used to estimate the intrinsic frequency. For $\omega_o << N$, assuming a single dominant wave, the intrinsic frequency depends on the ratio of the convergence $\nabla$ to the vorticity $\zeta$

$$\omega_o(k_z) = f \frac{\nabla(k_z)}{\zeta(k_z)} \quad . \tag{3}$$

Because of the similar treatment of vorticity and convergence, this estimate is more reliable than other intercomparisons that could be made. The intrinsic frequency is displayed as a function of vertical wavenumber in Fig. 13 for $\Delta r$=4 km. Where it falls below $\omega_o$, the model assumptions fail. For the variance-containing lower wavenumbers, the intrinsic frequencies lie between 1.2$f$ and 3$f$.

## SUMMARY AND CONCLUSIONS

Measurements were made in the vicinity of a seamount to look for ertel vorticity finestructure. Since the ertel vorticity of a fluid parcel can only be modified by irreversible processes, no ertel vorticity fluctuations are associated with internal gravity waves. Thus, finding ertel vorticity finestructure would be evidence of non-internal wave dynamics on the finescale, that is, stratified two-dimensional turbulence aka vortical mode (Riley *et al*, 1981; Lilly, 1983; Müller, 1984). We

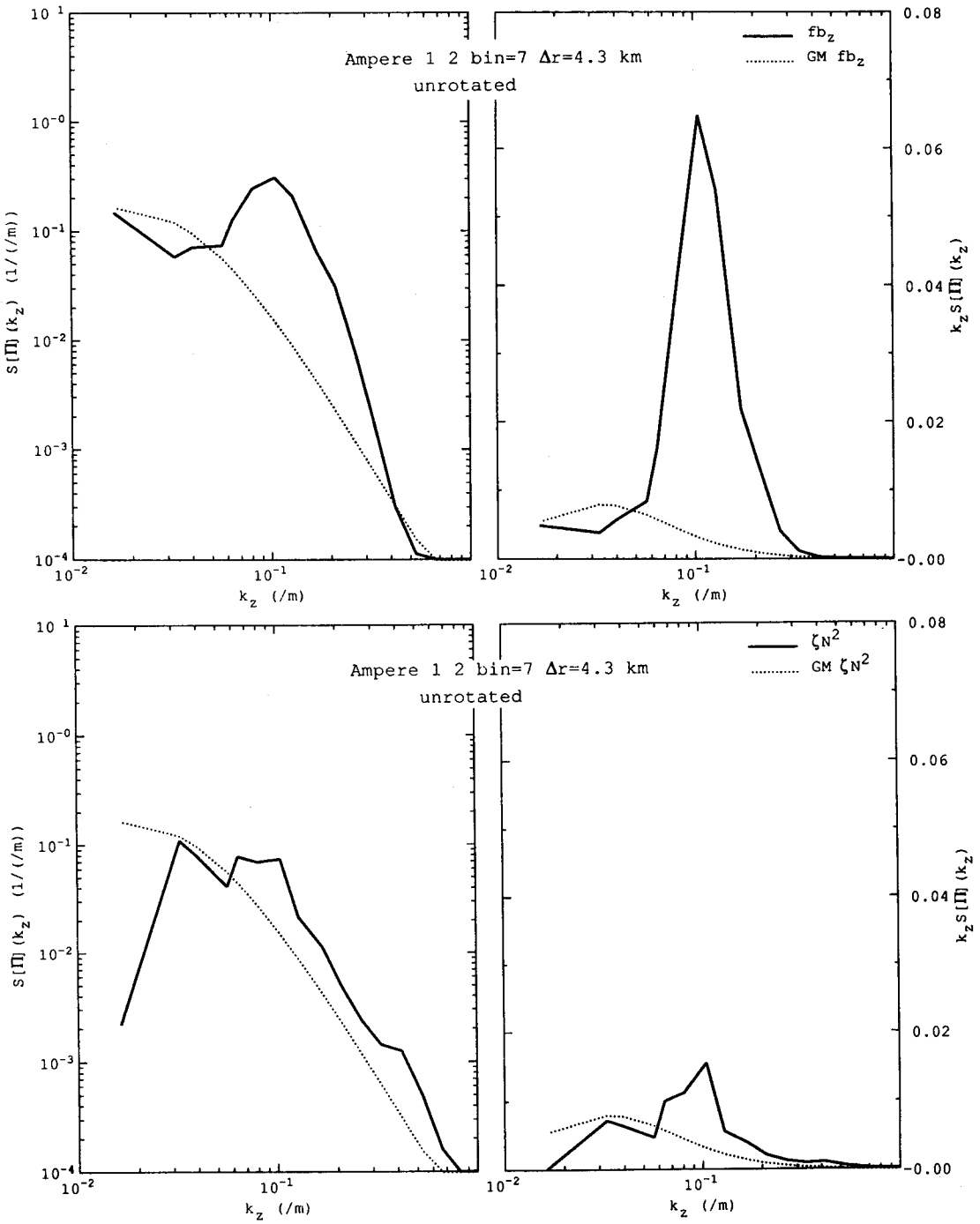


Figure 10. (a, top). Comparison of the vertical wavenumber spectrum for 4- km averaged stretching $fb_z$ from survey 1 with that from the GM internal wave model filtered to remove unresolved high horizontal wavenumbers ($k_H > \pi/\Delta r$). The observed stretching is higher than GM for $6\text{x}10^{-2}\text{m}^{-1}<k_z<2.5\text{x}10^{-1}$ m$^{-1}$. (b, bottom) Comparison of the vertical wavenumber spectrum for the 4-km fit vorticity $(v_x - u_y)\,\bar{N}^2$ from survey 1 with the GM internal wave model. Levels are comparable.

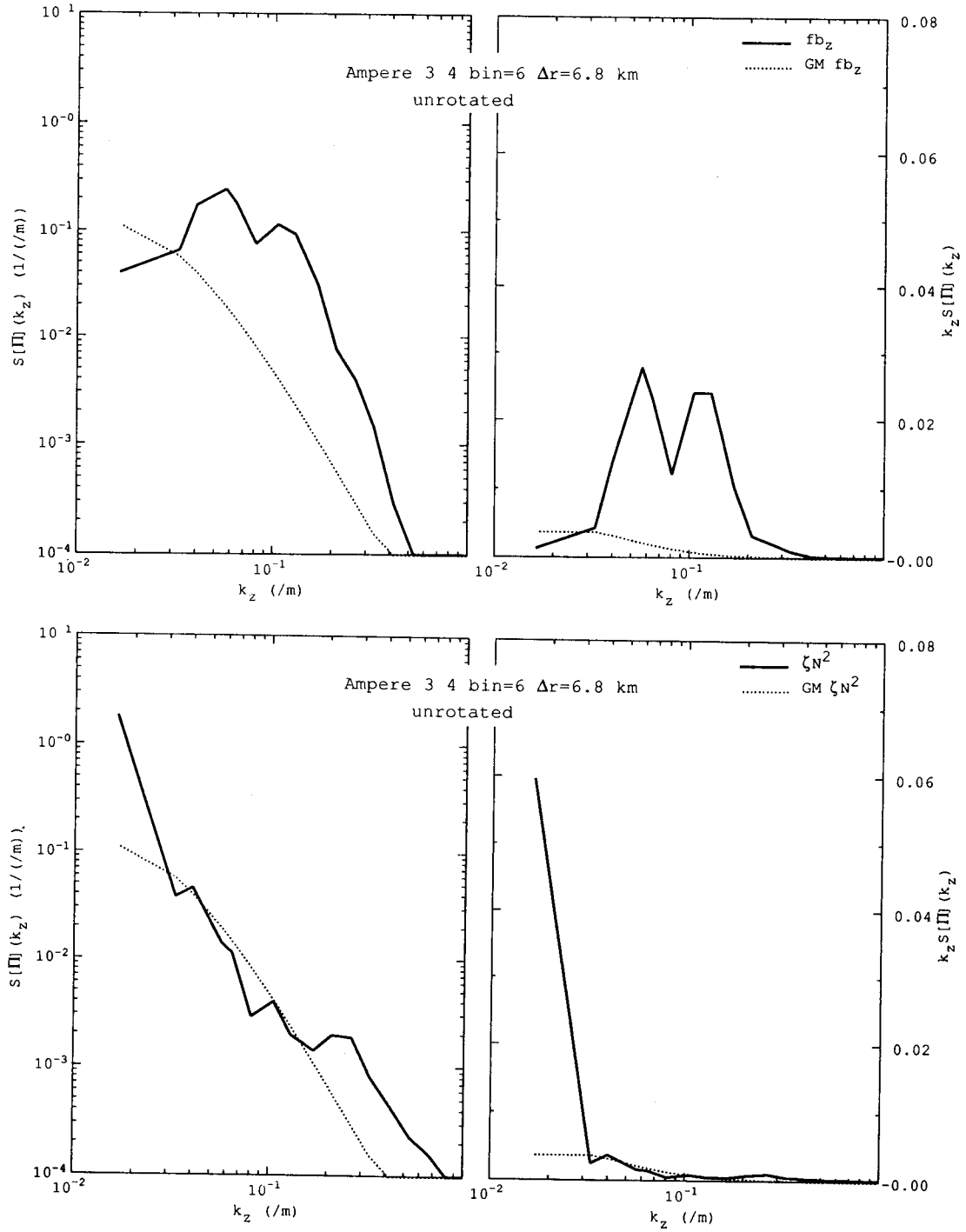


Figure 11. (a, top). As in Fig. 10a but for a 7-km fitting scale on survey 2. Again, observed stretching exceeds GM. (b, bottom) As in Fig. 10b but for a 7-km fitting scale on survey 2. Observed vorticity exceeds GM at the largest resolved wavelength ($\lambda_z$ = 384 m).

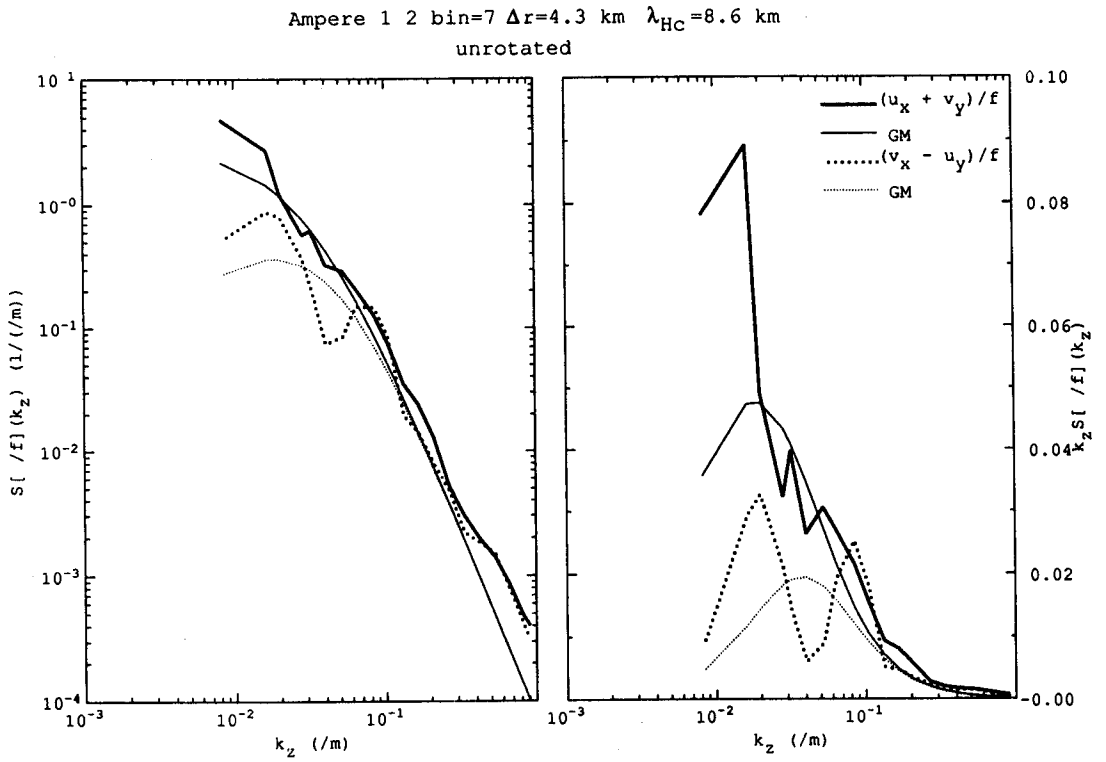
Ampere 1 2 bin=7 Δr=4.3 km λHc=8.6 km
unrotated
S[ /f](kz) (1/(/m))
kz (/m)
(ux + vy)/f
GM
(vx - uy)/f
GM
kzS[ /f](kz)

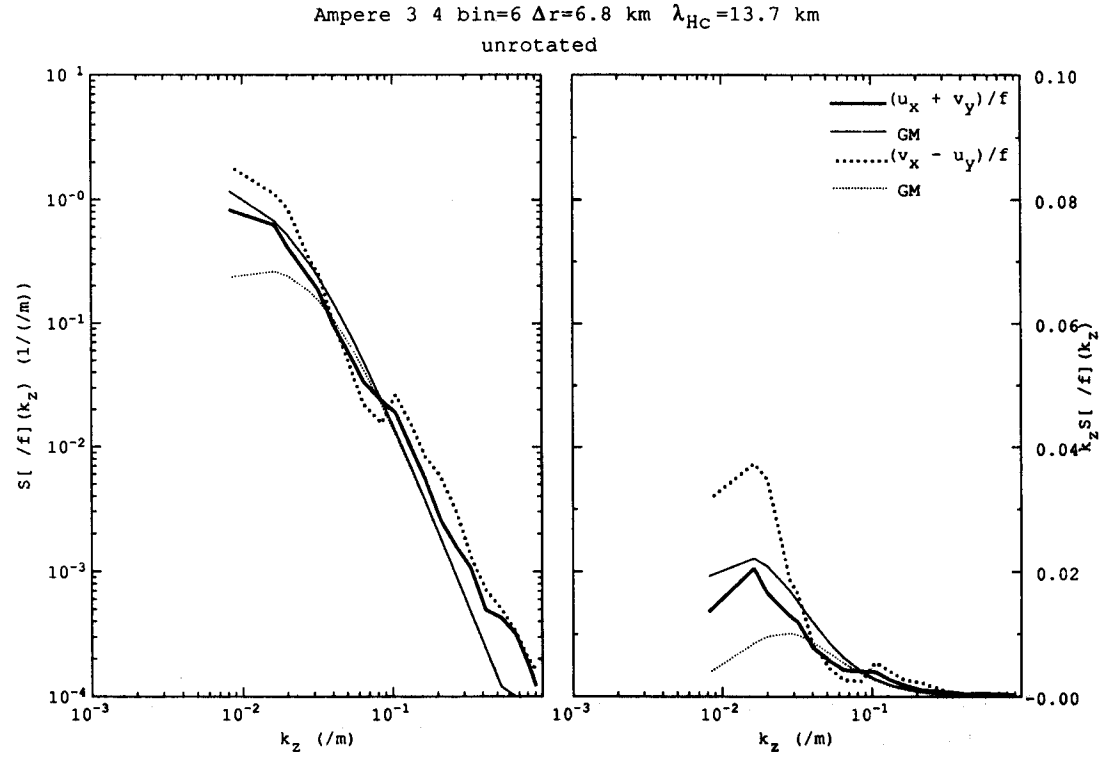
Ampere 3 4 bin=6 Δr=6.8 km λHc=13.7 km
unrotated
S[ /f](kz) (1/(/m))
kz (/m)
(ux + vy)/f
GM
(vx - uy)/f
GM
kzS[ /f](kz)

Figure 12a. (facing page, top). Comparison of the observed vertical wavenumber spectra for horizontal convergence and relative vorticity from survey 1 (thick curves) with the GM model integrated to horizontal wavenumbers of $\pi/8.6$ km $^{-1}$ (thin curves). This upper integration bound is consistent with the fitting scale of the horizontal gradients which filters out higher wavenumbers. Like the GM model, the observed convergence exceeds vorticity at low wavenumbers and is comparable at high wavenumbers. Also, the vorticity peaks at slightly higher wavenumbers than convergence in both measurements and model. This suggests that the dynamic (velocity) signal is dominated by internal waves.

Figure 12b. (facing page, bottom) As in Fig. 12a but for survey 2 and the GM model integrated to horizontal wavenumbers of $\pi/13.7$ km $^{-1}$. In this case, the observed vorticity slightly exceeds convergence at most wavenumbers, inconsistent with linear internal wave dynamics. The difference is small and may not be significant.

---

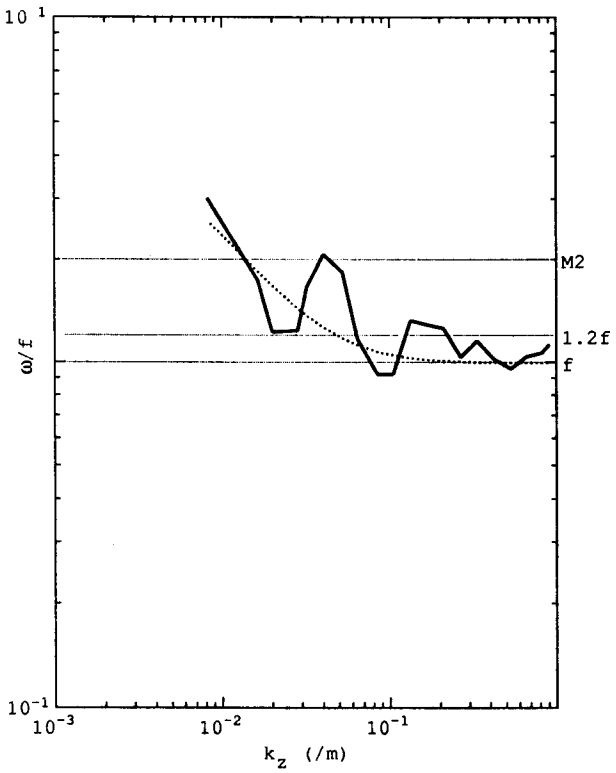


Figure 13. Intrinsic frequency versus vertical wavenumber as inferred from the ratio of horizontal convergence to relative vorticity (3) in survey 1 with $\Delta r$=4.3 km (thick solid) and the ratio of convergence to vorticity for the filtered GM model (dotted). This assumes a single internal wave dominates. Values below $f$ are inconsistent with (3). At variance-containing wavenumbers, values lie between 1.2-2.5$f$, consistent with the filtered GM model.

caution that the reverse is not true. An absence of ertel vorticity finestructure does not preclude the existence of stratified two-dimensional turbulence because vortices can have compensating contributions from the different terms (2) making up ertel vorticity (McWilliams, personal communication, 1991).

The velocity and temperature profile surveys described here reveal ertel vorticity finestructure on vertical wavelengths of 40-400 m and horizontal scales of 3-7 km near a seamount. As on basin scales, these scales are dominated by stretching $fb_z$. Thus, away from strong eddies, stretching can

be used to estimate ertel vorticity down to scales of a few kilometers. The implied high potential to horizontal kinetic energy ratio and low aspect ratios (see Fig. 1) are reminiscent of the density finestructure, aka pancake eddies or blini, discussed in the internal-wave literature in the early 70's (Phillips, 1971; Garrett and Munk, 1971; McKean, 1974; Eriksen, 1978; Levine and Irish, 1981). The stretching spectra peaks at ~60-m wavelength.

The dynamic (velocity) signal contains roughly equal amounts of relative vorticity $(v_x - u_y)/f$ and horizontal convergence $(u_x + v_y)/f$. For comparison, high-frequency internal waves have greater convergence than vorticity, near-inertial waves comparable convergence and vorticity, and stratified two-dimensional turbulence greater vorticity than convergence. Thus, the velocity signal is most consistent with near-inertial internal waves. This is borne out by the close agreement between the observed and GM vertical wavenumber spectra for these quantities at least in survey 1. With the exception of the $b_y u_z$ in survey 1 (Fig. 9a), the nonlinear vorticity and twisting contributions to the ertel vorticity, $(v_x - u_y)b_z$, $b_x v_z$ and $b_y u_z$, differ little from zero.

The velocity finescale being dominated by near-inertial waves is consistent with the findings of Kunze *et al.* (1990) and Sherman and Pinkel (1991). The dominance of the stretching term $fb_z$ in the ertel vorticity indicates that the observed anomalies are very nearly passive and geostrophic. This suggests that they were not recently formed by flow separation around Ampere Seamount since, in the near field, a wake of shed eddies should have a strong dynamic signal; flow separation at topography has been proposed as a generation mechanism for Arctic eddies (D'Asaro, 1988) and Meddies (Prater and Sanford, 1990) which have strong dynamic signals. Alternative explanations include:

- a signature of irreversible processes in the pycnocline.
- an artifact of subduction of surface mixed-layers or injection of benthic boundary layers from the flanks of Ampere Seamount (Armi, 1978).

As discussed in the introduction, the 60-m wavelengths of the finestructure are too large to be due to pycnocline turbulence given typical measured microstructure dissipation levels (Moum and Osborn, 1986; Gregg, 1987; Gregg, 1989; Yamazaki *et al.*, 1990). They are, however, similar to typical winter mixed-layer depths. Following subduction, vertically stacked mixed layers would slowly collapse and lose their dynamic signature (Gill, 1981). Dissipative turbulence and mixing concentrated at the base of the mixed layer would smear any pronounced sheet-and-layer structure, blending them into the background stratification. Alternatively, Nabatov and Ozmidov (1988) reported evidence of actively mixing layers in the pycnocline a few kilometers from Ampere Seamount. These layers appeared to have been generated by tidal advection of benthic boundary layers off the summit. While tidal advection would limit the excursion of the layers to within a few kilometers of the seamount, geostrophic flow like that we observe could carry them further. Emery (personal communication, 1991) and Roden (personal communication, 1991) have also found evidence of detached benthic boundary layers at the depth of the summit in the vicinity of Fieberling Guyot in the North Pacific. While our measurements indicate stretching ertel vorticity finestructure throughout the pycnocline, we cannot exclude this mechanism yet. We infer that the observed finestructure is not related to flow separation but is due to injection of mixed layers from either the

surface or benthic boundary. Additional analysis is needed to distinguish between these two boundary sources.

**Acknowledgments:** We would like to thank John Dunlap for his assistance in modifying Eric D'Asaro's XCP data acquisition program to acquire XBT data, Maureen Kennelly for handling the organization and logistics, Tom Lehman for the CTD work, and Captain Paul Howland and the crew of OCEANUS for their able assistance. This work was supported by ONR grant N00014-90-J-1100.

## REFERENCES

Armi, L, 1978: Some evidence of boundary mixing in the deep ocean. *J. Geophys. Res.*, **83**, 1971-1979.

Briscoe, M.G., 1977: On current finestructure and moored current-meter measurements of internal waves. *Deep-Sea Res.*, **24**, 1121-1131.

D'Asaro, E.A., 1988: Generation of submesoscale vortices: A new mechanism. *J. Geophys. Res.*, **93**, 6685-6693.

D'Asaro, E.A., and M.D. Morehead, 1991: Internal waves and velocity finestructure in the Arctic Ocean. *J. Geophys. Res.*, **96**, submitted.

Drever, R.G., and M.A. Kennelly, 1991: Design and use of a simple, low-cost drifter. in preparation.

Eriksen, C.C., 1978: Measurements and models of finestructure, internal gravity waves, and wave breaking in the deep ocean. *J. Geophys. Res.*, **83**, 2989-3009.

Ertel, H, 1942: Ein neuer hydrodynamischer Wirbelsatz. *Meteorol. Z.*, **59**, 277-281.

Garrett, C.J.R., and W. Munk, 1971: Internal wave spectra in the presence of finestructure. *J. Phys. Oceanogr.*, **1**, 196-202.

Garrett, C.J.R., and W. Munk, 1979: Internal waves in the ocean. *Ann. Rev. Fluid Mech.*, **11**, 339-369.

Gill, A.E., 1981: Homogeneous intrusions in a rotating stratified fluid. *J. Fluid Mech.*, **103**, 275-295.

Gregg, M.C., 1987: Diapycnal mixing in the thermocline: A review. *J. Geophys. Res.*, **92**, 5249-5286.

Gregg, M.C., 1989: Scaling turbulent dissipation in the thermocline. *J. Geophys. Res.*, **94**, 9686-9698.

Gregg, M.C., E.A. D'Asaro, T.J. Shay and N. Larson, 1986: Observations of persistent mixing and near-inertial internal waves. *J. Phys. Oceanogr.*, **16**, 856-885.

Haynes, P.H., and M.E. McIntyre, 1986: On the evolution of vorticity and potential vorticity in the presence of diabatic heating and frictional or other forces. *J. Atmos. Sci.*, **44**, 828-841.

Herring, J.A., and O. Metais, 1989: Numerical experiments in forced stably-stratified turbulence. *J. Fluid Mech.*, **202**, 97-115.

Holloway, G., 1983: A conjecture relating oceanic internal waves and small-scale processes. *Atmos.-Ocean*, **31**, 107-122.

Holloway, G., and D. Ramsden, 1989: Energy transfers by internal gravity wave interactions/stably stratified turbulence, presented at the *7th Conference on Atmospheric and Oceanic Waves and Stability*, Am. Meteorol. Soc., San Francisco, CA.

Itsweire, E.C., T.R. Osborn and T.P. Stanton, 1989: Horizontal distribution and characteristics of shear layers in the seasonal thermocline. *J. Phys. Oceanogr.*, **19**, 301-320.

Kunze, E., M.G. Briscoe, A.J. Williams III, 1990: Interpreting shear and strain finestructure from a neutrally-buoyant float. *J. Geophys. Res.*, **95**, 18,111-18,125.

Lelong, M.-P., and J.J. Riley, 1991: Internal wave-vortical mode interactions in strongly stratified flows. *J. Fluid Mech.*, submitted.

Levine, M.D., and J.D. Irish, 1981: A statistical description of temperature finestructure in the presence of internal waves. *J. Phys. Oceanogr.*, **11**, 676-691.

Lien, R.-C., 1990: Normal mode decomposition of small-scale oceanic motions. Ph.D. thesis, U of Hawaii, 128 pp.

Lilly, D.K., 1983: Stratified turbulence and the mesoscale variability of the atmosphere. *J. Atmos. Sci.*, **40**, 749-760.

Lin, J.-T., and Y.-H. Pao, 1979: Wakes in stratified fluids. *Ann. Rev. Fluid Mech.*, **11**, 317-338.

Marmorino, G.O., L.J. Rosenblum and C.L. Trump, 1987: Finescale temperature variability: The influence of near-inertial waves. *J. Geophys. Res.*, **92**, 13,049-13,062.

McKean, R.S., 1974: Interpretation of internal wave measurements in the presence of finestructure. *J. Phys. Oceanogr.*, **4**, 200-213.

McWilliams, J.C., 1989: Statistical properties of decaying geostrophic turbulence. *J. Fluid Mech.*, **198**, 199-230.

Metais, O., and J.R. Herring, 1989: Numerical simulations of freely evolving turbulence in stably stratified fluids. *J. Fluid Mech.*, **202**, 117-148.

Moum, J.N., and T.R. Osborn, 1986: Mixing in the main thermocline. *J. Phys. Oceanogr.*, **16**, 1250-1259.

Müller, P., 1984: Smallscale vortical motion, in *Internal Gravity Waves and Smallscale Turbulence, Proc. 'Aha Huliko'a Hawaiian Winter Workshop*, P. Müller and R. Pujalet, Eds., Hawaiian Inst. Geophys., Honolulu, 249-262.

Müller, P., D.J. Olbers and J. Willebrand, 1978: The IWEX spectrum. *J. Geophys. Res.*, **83**, 479-500.

Müller, P., R.-C. Lien and R. Williams, 1988: Estimates of potential vorticity at small scales in the ocean. *J. Phys. Oceanogr.*, **18**, 401-416.

Nabatov, V.N., and R.V. Ozmidov, 1988: Study of turbulence above seamounts in the Atlantic Ocean. *Oceanology*, **28**, 161-166.

Pedlosky, J., 1979: *Geophysical Fluid Dynamics*. Springer-Verlag, 624 pp.

Phillips, O.M., 1971: On spectra measured in an undulating layered medium. *J. Phys. Oceanogr.*, **1**, 1-6.

Prater, M.D., and T.B. Sanford, 1990: Generation of Meddies off Cape St. Vincent, Portugal. *EOS Transac., Amer. Geophys. Union*, **71**(43), 1416.

Riley, J.J., R.W. Metcalfe and M.A. Weissman, 1981: Direct numerical simulations of homogeneous turbulence in density-stratified fluids. in *Nonlinear Properties of Internal Waves*, 76, B.J. West, Ed., Amer. Inst. Phys., New York, 79-112.

Sherman, J.T., and R. Pinkel, 1991: Estimates of the vertical wavenumber-frequency spectra of vertical shear and strain. *J. Phys. Oceanogr.*, **21**, in press.

Staquet, C., and J.J. Riley, 1989: A numerical study of a stably-stratified mixing layer. *Turbulent Shear Flows*, **6**, Selected Pap. 6th Intl., Symp. 6th, 381-397.

Yamazaki, H., R.G. Lueck and T. Osborn, 1990: A comparison of turbulence data from a submarine and a vertical profiler. *J. Phys. Oceanogr.*, **20**, 1778-1786.